Fiber networks below the isostatic point: Fracture without stress concentration

Leyou Zhang, D. Zeb Rocklin, Leonard M. Sander, and Xiaoming Mao

Phys. Rev. Materials **1**, 052602 — Published 18 October 2017

DOI: 10.1103/PhysRevMaterials.1.052602

Fiber networks below the isostatic point: fracture without stress concentration

Leyou Zhang,[1] D. Zeb Rocklin,[1,2,3] Leonard M. Sander,[4] and Xiaoming Mao[1]

[1] *Department of Physics, University of Michigan, Ann Arbor, MI 48109-1040.*
[2] *Laboratory of Atomic and Solid State Physics, Cornell Univ., Ithaca, NY 14853-2501.*
[3] *School of Physics, Georgia Institute of Technology, Atlanta, Georgia 30332.*
[4] *Physics and Complex Systems, University of Michigan, Ann Arbor, MI 48109-1040.*

(Dated: October 2, 2017)

Crack nucleation, in which a crack is propagated via the concentration of stress at its tip, is a ubiquitous phenomenon. Here we show via simulations and theory that in systems such as fiber networks that are below the point of mechanical stability continuous nonlinear alignments lead to a steady state in which new load-bearing fiber chains emerge to replace those lost to fracture, preventing stress concentration and leading to accumulation of distributed damage over a divergent length scale. In contrast to linear models that display diverging length scales at a critical point, this phenomenon occurs over a large parameter range, and is expected to be observed in biopolymer networks and porous artificial materials. This mixture of fiber alignment and fracture leads to massively greater energy dissipation and to fracture avalanche statistics distinct from those present in linear models.

When brittle materials break, long straight cracks form; fracture occurs along roughly planar fracture surfaces (in dimension $d = 3$) or linear cracks ($d = 2$). A. Griffith[1] explained this through *stress concentration at the tips of the cracks*[2], leading to failure propagating along the cracks through large avalanches. In actual materials, disorder is always present, which lead to a process zone of size ξ over which the failure spreads and a wide distribution of avalanche sizes[3,4]. There are models with tunable disorder in which ξ can become large and even diverge at a critical point [5–9], leading to diffuse failure.

Systems such as biopolymer networks and certain artificial porous structures have an unusual type of disorder: they are composed of under-coordinated cross-linked fibers or thin elements. With central forces (stretching) alone, they would fall on the *unstable* side of a Central Force Isostatic Point (CFIP)[10–19]. When additional weak forces such as bending stiffness are present, the materials display nonlinear elasticity ("strain-stiffening") even when the constituent fibers are in the linear elastic regime[20–28]. Here we show that they have peculiar behavior under fracture: for an entire critical phase there is no remnant of a Griffith crack, and avalanches are always small.

We capture the failure of these systems below the CFIP using the diluted triangular lattice ($d = 2$) in which each bond is present with probability p (Fig. 1)[16,17,24,25,29–31]. Consecutive bonds along a straight line are identified as a fiber, with average length $1/(1-p)$ (bond length taken to be 1), and nodes in the lattice are identified as free-hinging crosslinks. Elastic energy of the network includes stretching and bending of the fibers: each existing bond is a harmonic spring of spring constant k, and two adjacent bonds along a fiber contribute bending energy $\kappa\theta^2/2$. We focus on $\kappa/k \ll 1$, appropriate for biopolymers such as collagen-I with ratio $\approx 10^{-5}$.

At the CFIP the degrees of freedom (d per node) and central force constraints (1 per bond) are equal, and the system is at the verge of mechanical instability. This implies an average coordination number $\langle z\rangle = 2d$ and hence $p = 2/3$[10–19], close to the measured central-force rigidity percolation point $p_c \simeq 0.6602$[11]. All fiber networks with two fibers meet at a crosslink are below the CFIP ($\langle z\rangle < 2d$), and their linear elastic moduli are determined by bending stiffness κ[30]. At large strain bonds rotate and align to bear external stress in new ways, the network enters the stretching dominated regime, the mechanism to which strain-stiffening in real biopolymers such as collagen-I[20,23] is attributed.

We focus on fracture *below* the CFIP ($\langle z\rangle < 2d$), in which bonds break only after nonlinear strain stiffening, so the entire process is controlled by the formation of the force chains. We find the system showing remarkable behavior for very small κ: in the *finite* parameter range $\langle z\rangle < 2d$ (but substantially above geometric percolation), the process zone $\xi \to \infty$, and the network shows diffuse failure even in the thermodynamic limit. The system is so disordered that the Griffith scenario of breaking near a crack tip is never relevant. Stress concentration is overwhelmed by disorder.

We construct our network by starting with an $L \times L$ triangular lattice with each bond present with probability p and elastic energy as discussed above. Each bond is a linear spring of spring constant k until, at common strain threshold $\lambda = .03$, the bond breaks and removes its stretching and bending energies. Our model shares similarities with the RFM[5,6,32] in terms of introducing randomness in a lattice model. However, in contrast to our natural geometric disorder, the RFM[5,6] has disorder in λ with a prescribed distribution. We will investigate a close relationship between the RFM and our model below.

We apply a uniaxial strain $u_{yy} = \gamma$ and minimize the system's elastic energy using the FIRE algorithm[33]. Periodic boundary conditions are applied for the x-direction, while the top and bottom boundaries are held as rigid bars to impose strain. Nodes are allowed to slide along the bars. We apply strain in small steps such that only

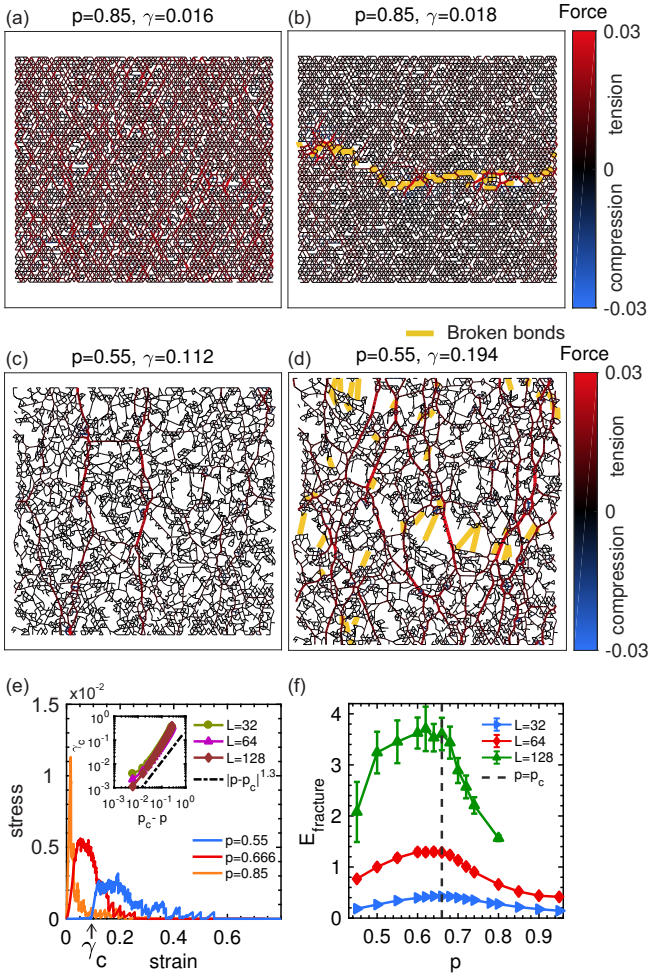

FIG. 1. (Color online) (a) Stress concentration near crack tips in dense fiber networks above the CFIP, with the resulting Griffith crack shown in (b). (c) and (d) show force chains and diffuse failure in dilute fiber networks below the CFIP. Bonds are colored according to force; broken bonds are also marked (see legend). Bonds with larger force are thicker. (e) Stress-strain curves at various p for $L = 128$. The critical strain, γ_c, is labeled for $p = 0.55$. Inset: Scaling relation $\gamma_c \sim (p_c - p)^\beta$ with $\beta \simeq 1.3$[25], for different L. (f) The fracture energy reaches a maximum when $p \simeq p_c$.

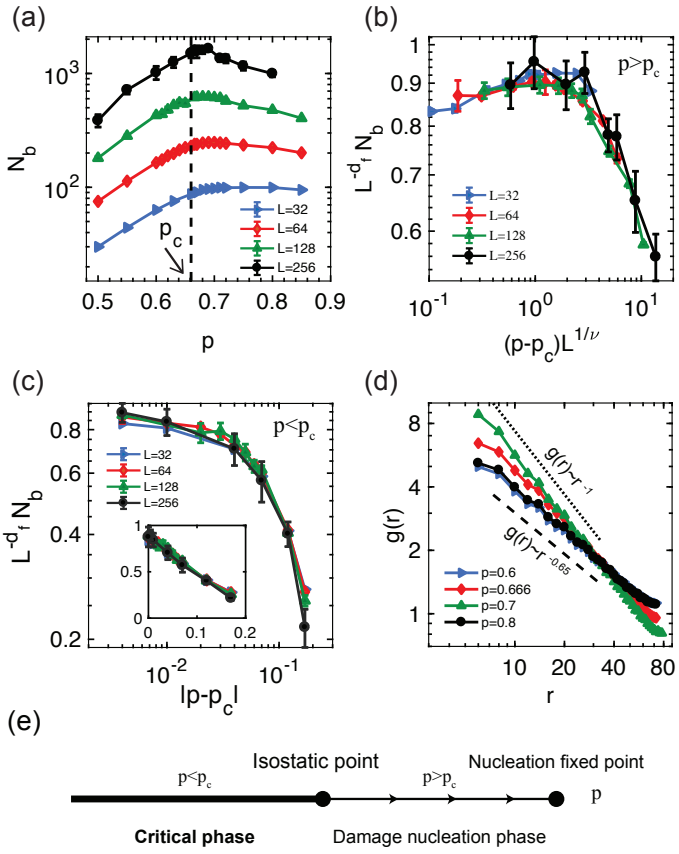

FIG. 2. (Color online) (a) N_b as a function of p for $L = 32, 64, 128, 256$, displaying a maximum at p_c. (b) Scaling of N_b for $p > p_c$ with $\nu = 1.21$. (c) Scaling of N_b for $p < p_c$ with $\nu \to \infty$. Inset: The same plot in a linear-linear scale. (d) The pair correlation function $g(r)$ of broken bonds at $L = 128$. (e) Schematic phase diagram with arrows showing the direction of flow as $L \to \infty$.

one bond initially breaks, but that breakage can trigger an avalanche as stress redistributes itself. Once the avalanche terminates, the system is further strained, continuing until the lattice is broken into two disconnected pieces (final failure). A small notch of 8 broken bonds is placed in the center of the lattice to nucleate a crack. We focus on $\kappa = 0$, in which strain stiffening is most pronounced; as we will see small κ leaves the nonlinear fracture physics qualitatively unchanged.

Results are shown in Fig. 1(a-d) for $\kappa = 0$. For $p > p_c$ the network is well described by Griffith theory. When $p < p_c$, the system is bending dominated at small strain (elastic moduli proportional to κ), until the strain-stiffening critical strain $\gamma_c \sim (p_c - p)^\beta$ with $\beta \simeq 1.3$[25]. Beyond γ_c bonds start to be stretched and will break when they extend beyond the threshold length; see Fig. 1(c-e). The total energy absorbed during the fracturing process, the fracture energy (the area under the stress-strain curve), as shown in Fig. 1(f), peaks at $p \simeq p_c$. Networks close to the CFIP display highest toughness.

To extract ξ, we use a finite-size scaling form for the total number of broken bonds, N_b, at failure (Fig. 2). Clearly, $N_b \sim L$ as $p \to 1$ (crack nucleation) and $N_b \to 0$ as $p \to p_{GP} \simeq 0.347$ (geometric percolation[34]). Close to the CFIP the data can be collapsed using:

$$N_b = L^{d_f} \mathcal{N}\left(|p - p_c| L^{1/\nu}\right), \qquad (1)$$

with $d_f = 1.35$. We find a good collapse for $p > p_c$ using $\nu = 1.21$, the value from rigidity percolation[11,35] [Fig. 2(b)], consistent with a correlation length $\xi \sim |p - p_c|^{-\nu}$. The physical meaning of ξ in rigidity percolation is the scale at which the probability for a network being rigid exhibits significant fluctuations. Here it controls the size of the process zone, because below this scale stress

cannot be concentrated at the crack tip. This agrees with previous results from linear simulations as the CFIP is approached from above[9] (although a different exponent ν was found for the different network architecture). In the random fuse model (RFM), the divergence of ξ occurs at infinite disorder in the fuse thresholds[7,8,32]. In both $p > p_c$ networks and the RFM the systems flow to the nucleation fixed point when $L \gg \xi$.

In sharp contrast, for $p < p_c$ (below the CFIP), the data collapses using $\nu \to \infty$, Fig. 2(c), i.e., an infinite correlation length for the process zone. Networks below the CFIP break when the strain exceeds γ_c (onset of strain stiffening), deep in the regime of nonlinear elasticity. Instead of nucleation, a dynamic steady state emerges during fracture, with force chains continuously emerging throughout the system as other chains break and the network strains. Because of nonlinear alignments, fiber networks below the CFIP organize into a state that resembles the critical CFIP throughout the entire fracture process. Furthermore, for $p < p_c$ the scaling function $\mathcal{N}$ takes the linear form $\mathcal{N}(y) = a_1 - a_2 y$ where $a_1 \simeq 0.9$ and $a_2 \simeq 3.8$ are constants. Because the energy dissipated by fracture is proportional to the bonds broken in Eq. (1), this process dramatically increases the fracture toughness of the network.

We interpret the exponent $d_f = 1.35$ as the fractal dimension of the cluster of broken bonds in the process zone. To verify this we measured the pair correlation function $g(r)$ [Fig. 2(d)]. For $p < p_c$ the process zone is the whole lattice and we observe $g(r) \sim r^{d_f - 2}$. This crosses over to $g(r) \sim r^{-1}$ for $p \to 1$ as a result of crack nucleation. To get $g(r)$ we used the positions of the broken bonds in the undeformed state and we disregard the first 20% of broken bonds for $p < p_c$ to eliminate uncorrelated damage at the beginning[36,37].

Our scaling collapse of N_b shows that for $p > p_c$ the system always flows to the nucleation fixed point as L/ξ increases, whereas for $p < p_c$ the system does not flow ($\xi \to \infty$). Rather it drives itself to the CFIP in the nonlinear regime during fracture. We call this regime the "critical phase" [see phase diagram in Fig. 2(e)]. This is similar to the phenomenon of molecular motors driving biopolymer gels to a critically connected state[38].

We now consider the effect of increasing κ from 0, which gives the lattice a small rigidity in linear regime. Using simulation we verify that the same physics of diffuse failure applies when $\kappa \ll k$, whereas in the opposite limit of large bending stiffness, $\kappa \sim k$, Griffith theory applies [Fig. 3]. We find that N_b plateaus in the limit of $\kappa \to 0$ [Fig. 3(b) inset].

We also studied the integrated size distribution $D_{int}(s, p, L)$ for all avalanches of size s until failure (at $\kappa = 0$). A standard form[3,36,39] is $D_{int}(s, p, L) = s^{-\tau}\mathcal{D}(s/s_0)$; s_0 is a cutoff size for the power law $s^{-\tau}$. As shown in Fig. 4(a) for our model $\tau = 3/2$. The cutoff size s_0 is a function of p and L, and the scaling we obtained above, $\xi \sim |p - p_c|^{-\nu}$, provides a way to collapse

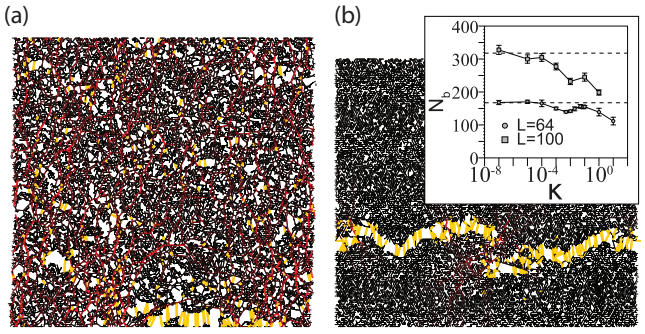

FIG. 3. (Color online) (a) Diffuse failure at small bending stiffness $\kappa = 10^{-4}$. (b) Griffith crack at $\kappa = 10^{-1}$. $L = 128$, $p = 0.6$. Color coding same as in Fig. 1. Inset in (b) shows N_b vs κ at two system sizes. As $\kappa \to 0$, N_b plateaus toward the $\kappa = 0$ limit [dashed lines, upper $L = 100$, lower $L = 64$].

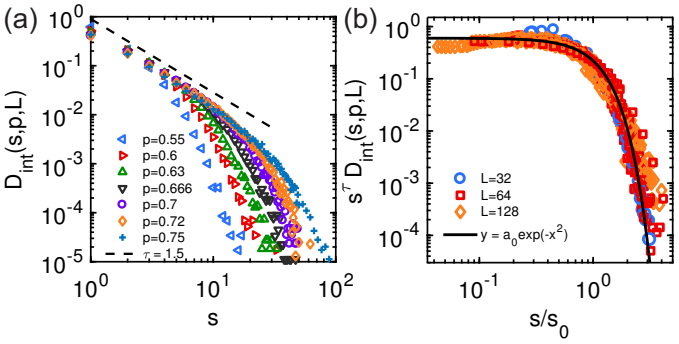

FIG. 4. (Color online) (a) Integrated avalanche size distribution $D_{int}(s, p, L)$ at $L = 128$, various p. Dashed line: the power law $s^{-\tau}$, $\tau = 1.5$. (b) The collapse of $D_{int}(s, p, L)$ for $L = 32, 64, 128$ and p values as listed in (a), following Eq.(2). Solid line: empirical function that fits the master curve.

$D_{int}(s, p, L)$ onto a master curve (Fig. 4b):

$$s_0(p, L) = L^D \mathcal{S}(|p - p_c| L^{1/\nu}). \qquad (2)$$

Our data is consistent with $D \approx 1$. This should be compared to the RFM[36,40] for which $D \approx 1.1$. Also, $\mathcal{S}(x) = c_0 + c_1 x$ for $p > p_c$ and $\mathcal{S}(x) = c_0 + c_2 x$ for $p < p_c$, where $c_0 \simeq 0.11$, $c_1 \simeq 0.024$, and $c_2 \simeq -6.1$. We have used the correlation length exponent we obtained above, $\nu = 1.21$ for $p > p_c$ and $\nu \to \infty$ for $p < p_c$. This collapse is consistent with our interpretation of ξ.

To provide an intuitive picture for the force chain forming-breaking steady state and for $\tau = 3/2$, we introduce a toy model, the "slack fiber bundle model" (SFBM, see Fig. 5a) inspired by the fiber bundle model (FBM) for fracture with random breaking thresholds (as in the RFM)[3,41,42]. In the FBM, two plates are connected by fibers of random strengths. The plates are pulled apart with force F, which is equally shared by all fibers. Avalanches can occur where the breaking of one fiber makes others break. The avalanche size distribution is equivalent to the first return time of a biased random walk[41,43], $D^{FBM}(s, F) \sim s^{-3/2} e^{-s/s_0(F)}$,

where the bias (the ratio between mean and variance) is $b = s_0(F)^{-1/2} \sim F_c - F$, where F_c is the critical force where the final catastrophic failure occurs. The integrated avalanche distribution over the whole process is: $D_{int}^{FBM}(s) \sim \int_0^{F_c} D^{FBM}(s,F)dF \sim s^{-5/2}$. The 5/2 exponent is the result of vanishing bias (divergent cutoff s_0) as the final failure is approached [see Fig. 5(b)][44], and is characteristic of most brittle fracture processes.

In the SFBM, instead of a distribution of the threshold, we assume a distribution of fibers' rest length, $P(x_0)$, and assume that the fiber will break when it is stretched beyond $(1+\lambda)x_0$. Thus, the load F is not equally shared by all fibers. Instead, fibers with rest length longer than the distance between the plates remain slack until the distance between plates increases to their x_0. In this model (as in the original 2D network) new force chains constantly emerge in the process of failure. We assume the distribution of x_0 is quite random, i.e. the standard deviation is comparable to the mean. It is shown in detail in[44] that the bias in the random walk of force is a constant (Fig. 5b), $s_0^{-1/2} \sim \lambda$, when $\lambda \ll 1$, so that only a small fraction of the fibers are stretched at any given force. The integrated avalanche size distribution is:

$$D_{int}^{SFBM}(s) \sim \int_0^{F_c} D^{SFBM}(s,F)dF \sim s^{-3/2}e^{-\frac{\lambda^2 s}{2}}. \quad (3)$$

Failure in the SFBM is a steady state where new fibers join the load-bearing group and ones beyond threshold break. This steady-state process with $\tau = 3/2$ is reminiscent of other mean-field "self-organized branching processes" such as plastic slip events[45–47]. In contrast, in the FBM, all of the fibers are stretched, and the fracture process evolves significantly, culminating in a catastrophic failure.

The SFBM crosses over to FBM behavior when $\lambda \gtrsim 1$. In this case, a macroscopic fraction of the fibers are stretched at the same time, the distribution of rest length is overwhelmed by the distribution of the threshold, and the avalanches are like those in the FBM. We find that in the SFBM, taking large λ leads to a crossover from $\tau = 3/2$ to 5/2 (Fig. 5c). The same phenomena occur in the fiber networks as well, as shown in Fig. 5(d). With large λ the exponent is 5/2, and we have localized crack nucleation, destroying the critical phase for $p < p_c$.

In summary, we have shown via simulations and exact results that fiber networks, *for a finite range of connectivity below the CFIP*, exhibit a remarkable fracture process deep in the nonlinear elasticity regime, where force chains steadily emerge and break, stress never concentrate, and the size of the process zone is divergent.

Our results may apply to failure of some real biopolymer gels, a question that is important in characterizing tissue failure[48–50], provided that the the bending stiffness is small, the network is mainly athermal, and the failure of the individual polymer does not involve complicated macromolecular structures[51]. Deviations from this simple limit will likely drive the network to focus stress and crossover to crack nucleation in the thermodynamic limit.

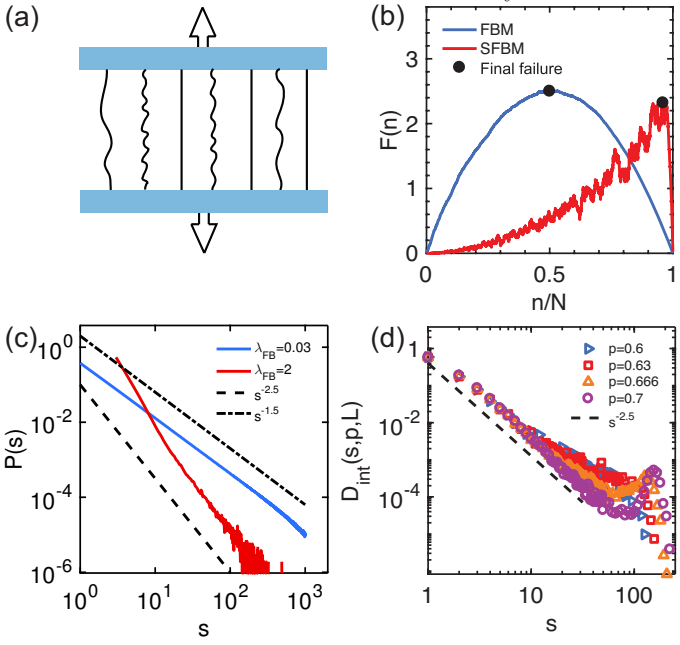

FIG. 5. (a) SFBM schematic. (b) Force as a function of number of broken fibers in FBM and SFBM. (c) Crossover of τ in the SFBM with λ. (d) $D_{int}(s,p,L)$ at $\lambda = 0.2$ and various p for the fiber network model at $L = 128$.

Furthermore, diverse hybrid materials, from hydrogels[52] to bone[53,54], possess not only strong bonds capable of bearing great stress, but also "sacrificial bonds"[55] that break and unspool hidden length, increasing the material's toughness as measured in its ability to absorb and dissipate energy. Our simple, non-hybrid materials exploit nonlinear alignments to spontaneously form "sacrificial bonds" that dissipate energy while also undergoing great strain. Unlike conventional cracks which dissipate energy proportional to a material's cross-section, the distributed damage has, in our simulations, fractal dimension 1.35 in dimension 2, a fundamentally distinct structure which leads to greater damage distribution. Counter to intuition, this toughening is achieved by *removing* material to improve flexibility and allow the system to bear distribute stress more efficiently.

Acknowledgments We acknowledge informative discussions with James Sethna. This work was supported in part by the National Science Foundation Grant No. NSF DMR-1609051 (XM and LZ), the ICAM postdoctoral fellowship, the Bethe/KIC Fellowship, and the National Science Foundation Grant No. NSF DMR-1308089 (DZR).

[1] A. A. Griffith, Philosophical transactions of the royal society of london. Series A, containing papers of a mathematical or physical character **221**, 163 (1921).
[2] G. R. Irwin, Journal of Applied Mechanics **24**, 361 (1957).
[3] M. J. Alava, P. K. Nukala, and S. Zapperi, Advances in Physics **55**, 349 (2006).
[4] D. Bonamy and E. Bouchaud, Physics Reports **498**, 1 (2011).
[5] S. Roux, A. Hansen, H. Herrmann, and E. Guyon, Journal of statistical physics **52**, 237 (1988).
[6] A. Hansen and J. Schmittbuhl, Phys. Rev. Lett. **90**, 045504 (2003).
[7] M. J. Alava, P. K. V. V. Nukala, and S. Zapperi, Phys. Rev. Lett. **100**, 055502 (2008).
[8] A. Shekhawat, S. Zapperi, and J. P. Sethna, Phys. Rev. Lett. **110**, 185505 (2013).
[9] M. M. Driscoll, B. G.-g. Chen, T. H. Beuman, S. Ulrich, S. R. Nagel, and V. Vitelli, Proceedings of the National Academy of Sciences **113**, 10813 (2016).
[10] J. C. Maxwell, Philos. Mag. **27**, 294 (1864).
[11] D. J. Jacobs and M. F. Thorpe, Phys. Rev. Lett. **75**, 4051 (1995).
[12] M. Wyart, Ann. Phys. Fr **30**, 1 (2005).
[13] X. Mao, N. Xu, and T. C. Lubensky, Phys. Rev. Lett. **104**, 085504 (2010).
[14] X. Mao and T. C. Lubensky, Phys. Rev. E **83**, 011111 (2011).
[15] W. G. Ellenbroek and X. Mao, Europhys. Lett. **96** (2011).
[16] X. Mao, O. Stenull, and T. C. Lubensky, Phys. Rev. E **87**, 042601 (2013).
[17] X. Mao, O. Stenull, and T. C. Lubensky, Phys. Rev. E **87**, 042602 (2013).
[18] T. C. Lubensky, C. Kane, X. Mao, A. Souslov, and K. Sun, Reports on Progress in Physics **78**, 073901 (2015).
[19] L. Zhang, D. Z. Rocklin, B. G.-g. Chen, and X. Mao, Phys. Rev. E **91**, 032124 (2015).
[20] P. R. Onck, T. Koeman, T. van Dillen, and E. van der Giessen, Phys. Rev. Lett. **95**, 178102 (2005).
[21] M. Gardel, J. Shin, F. MacKintosh, L. Mahadevan, P. Matsudaira, and D. Weitz, Science **304**, 1301 (2004).
[22] D. Vader, A. Kabla, D. Weitz, and L. Mahadevan, PloS one **4**, e5902 (2009).
[23] C. P. Broedersz and F. C. MacKintosh, Reviews of Modern Physics **86**, 995 (2014).
[24] J. Feng, H. Levine, X. Mao, and L. M. Sander, Physical Review E **91**, 042710 (2015).
[25] J. Feng, H. Levine, X. Mao, and L. M. Sander, Soft matter **12**, 1419 (2016).
[26] A. J. Licup, S. Münster, A. Sharma, M. Sheinman, L. M. Jawerth, B. Fabry, D. A. Weitz, and F. C. MacKintosh, Proceedings of the National Academy of Sciences **112**, 9573 (2015).
[27] G. Žagar, P. R. Onck, and E. van der Giessen, Biophysical journal **108**, 1470 (2015).
[28] A. Sharma, A. Licup, K. Jansen, R. Rens, M. Sheinman, G. Koenderink, and F. MacKintosh, Nature Physics **12**, 584 (2016).
[29] M. Das, F. C. MacKintosh, and A. J. Levine, Phys. Rev. Lett. **99**, 038101 (2007).
[30] C. P. Broedersz, X. Mao, T. C. Lubensky, and F. C. MacKintosh, Nat. Phys. **7**, 983 (2011).
[31] P. Duxbury and S. Kim, in *MRS Proceedings*, Vol. 207 (Cambridge Univ Press, 1990) p. 179.
[32] A. Hansen, E. L. Hinrichsen, and S. Roux, Phys. Rev. B **43**, 665 (1991).
[33] E. Bitzek, P. Koskinen, F. Gähler, M. Moseler, and P. Gumbsch, Phys. Rev. Lett. **97**, 170201 (2006).
[34] M. F. Sykes and J. W. Essam, Journal of Mathematical Physics **5**, 1117 (1964).
[35] D. J. Jacobs and M. F. Thorpe, Phys. Rev. E **53**, 3682 (1996).
[36] P. K. V. V. Nukala, S. Zapperi, and S. Šimunović, Phys. Rev. E **71**, 066106 (2005).
[37] P. K. V. V. Nukala, S. Šimunović, and S. Zapperi, Journal of Statistical Mechanics: Theory and Experiment **2004**, P08001 (2004).
[38] J. Alvarado, M. Sheinman, A. Sharma, F. C. MacKintosh, and G. H. Koenderink, Nature Physics **9**, 591 (2013).
[39] J. P. Sethna, K. A. Dahmen, and C. R. Myers, Nature **410**, 242 (2001).
[40] L. de Arcangelis and H. J. Herrmann, Phys. Rev. B **39**, 2678 (1989).
[41] P. C. Hemmer and A. Hansen, Journal of applied mechanics **59**, 909 (1992).
[42] S. Pradhan, A. Hansen, and B. K. Chakrabarti, Reviews of modern physics **82**, 499 (2010).
[43] D. Sornette, Journal de Physique I **2**, 2089 (1992).
[44] See Supplemental Material at [URL will be inserted by publisher] for a detailed discussion of the SFBM..
[45] S. Zapperi, K. B. Lauritsen, and H. E. Stanley, Physical review letters **75**, 4071 (1995).
[46] K. A. Dahmen, Y. Ben-Zion, and J. T. Uhl, Physical review letters **102**, 175501 (2009).
[47] K. A. Dahmen, Y. Ben-Zion, and J. T. Uhl, Nature Physics **7**, 554 (2011).
[48] M. C. Ritter, R. Jesudason, A. Majumdar, D. Stamenović, J. A. Buczek-Thomas, P. J. Stone, M. A. Nugent, and B. Suki, Proceedings of the National Academy of Sciences **106**, 1081 (2009).
[49] X. Wei, Q. Zhu, J. Qian, Y. Lin, and V. Shenoy, Soft matter **12**, 2537 (2016).
[50] M. Ovaska, Z. Bertalan, A. Miksic, M. Sugni, C. Di Benedetto, C. Ferrario, L. Leggio, L. Guidetti, M. J. Alava, C. A. La Porta, *et al.*, Journal of the Mechanical Behavior of Biomedical Materials **65**, 42 (2017).
[51] M. J. Buehler, Proceedings of the National Academy of Sciences **103**, 12285 (2006).
[52] J.-Y. Sun, X. Zhao, W. R. Illeperuma, O. Chaudhuri, K. H. Oh, D. J. Mooney, J. J. Vlassak, and Z. Suo, Nature **489**, 133 (2012).
[53] J. B. Thompson, J. H. Kindt, B. Drake, H. G. Hansma, D. E. Morse, and P. K. Hansma, Nature **414**, 773 (2001).
[54] G. E. Fantner, T. Hassenkam, J. H. Kindt, J. C. Weaver, H. Birkedal, L. Pechenik, J. A. Cutroni, G. A. Cidade, G. D. Stucky, D. E. Morse, *et al.*, Nature Materials **4**, 612 (2005).
[55] J. Currey, Nature **414**, 699 (2001).